Journal of Neuroscience Methods 176 (2009) 129–135

Contents lists available at ScienceDirect

Journal of Neuroscience Methods

journal homepage: www.elsevier.com/locate/jneumeth

PET measurement of changes in D2/D3 dopamine receptor binding in a nonhuman primate during chronic deep brain stimulation of the bed nucleus of the stria terminalis

Nicholas T. Vandehey[a], P. Charles Garell[b], Joseph A. Hampel[c], Dhanabalan Murali[c], Elizabeth M. Smith[a], Richard Davidson[c], Alexander K. Converse[c], R. Jerry Nickles[a], Bradley T. Christian[a,c,*]

[a] University of Wisconsin-Madison, Department of Medical Physics, United States
[b] New York Medical College, Department of Neurosurgery, United States
[c] University of Wisconsin-Madison, Waisman Laboratory for Brain Imaging and Behavior, United States

ARTICLE INFO

Article history:
Received 21 April 2008
Received in revised form 27 August 2008
Accepted 27 August 2008

Keywords:
Deep brain stimulation
DBS
PET
BNST
D2/D3
Dopamine
Fallypride

ABSTRACT

PET imaging is a powerful tool for measuring physiological changes in the brain during deep brain stimulation (DBS). In this work, we acquired five PET scans using a highly selective D2/D3 dopamine antagonist, 18F-fallypride, to track changes in dopamine receptor availability, as measured by the distribution volume ratio (DVR), through the course of DBS in the bed nucleus of the stria terminalis (BNST) in a nonhuman primate.

Methods: PET scans were performed on a rhesus monkey with unilateral BNST stimulation during periods of baseline, chronic high frequency (130 Hz) and low frequency (50 Hz) DBS stimulation, and during a washout period between stimulation periods. A final scan was performed with the electrode stimulation starting 110 min into the scan. Whole brain parametric images of ^{18}F-fallypride DVR were calculated for each condition to track changes in both striatal and extrastriatal D2/D3 availability.

Results: The monkey displayed significant increases in receptor binding throughout the brain during DBS relative to baseline for 130 and 50 Hz, with changes in DVR of: caudate 42%, 51%; putamen 56%, 57%; thalamus 33%, 49%; substantia nigra 29%, 26%; and prefrontal cortex 28%, 56%, respectively. Washout and post-stimulation scans revealed DVR values close to baseline values. Activating the stimulator midway through the final scan resulted in no statistically significant changes in binding.

Conclusions: PET neuroligand imaging has demonstrated the sensitivity to track changes in dopamine D2/D3 binding during the course of DBS. These methods show great potential for providing insight into the neurochemical consequences of DBS.

1. Introduction

Deep brain stimulation (DBS) of the subthalamic nucleus, globus pallidus or thalamus are clinically used methods for effective alleviation of symptoms associated with movement disorders such as Parkinson's disease, essential tremor, and dystonia. DBS has also been used experimentally in attempts to treat epilepsy, depression, obsessive–compulsive disorder, cluster headache, and most recently, obesity (Leone et al., 2005; Mayberg et al., 2005; Perlmutter and Mink, 2006; Sani et al., 2007; Lacan et al., 2008; Hamani et al., 2008). Despite its many uses, the mechanisms of DBS effectiveness remain unclear (McIntyre et al., 2004; Montgomery and Gale, 2008). Much of the current research in DBS uses electrical recording on the cellular level, but a more systems level approach, such as molecular imaging, shows promise as a research tool for understanding the neurochemical changes accompanying DBS treatment.

Functional imaging using positron emission tomography (PET) has been used to investigate the effects of DBS in a variety of experiments. Using ^{15}O–H_2O as a tracer to measure changes in regional blood flow in essential tremor patients, Perlmutter et al. (2002) found that thalamic stimulation increased blood flow in targets downstream of the thalamus. Also using ^{15}O–H_2O, Haslinger et al. (2005) examined patients with DBS of the ventralis intermedius,

* Corresponding author at: University of Wisconsin-Madison, T235 Waisman Center, 1500 Highland Avenue, Madison, WI 53705, United States.
Tel.: +1 608 890 0750.
E-mail address: bchristian@wisc.edu (B.T. Christian).

0165-0270/$ – see front matter © 2008 Elsevier B.V. All rights reserved.
doi:10.1016/j.jneumeth.2008.08.033

measuring increases in blood flow at the stimulation site and sensory motor cortex, both correlated with stimulus frequency and stimulus amplitude. Other PET research has used ^{18}F-FDG to measure regional metabolism during DBS. Fukuda et al. (2001) observed metabolic changes correlated with changes in the Unified Parkinsons Disease Rating Scale scores during pallidal DBS, while Hilker et al. (2004) found that DBS of the subthalamic nucleus activates the stimulated target while altering non-motor circuits. Furthermore, the experiments by Schlaepfer et al. (2007) showed that DBS of the nucleus accumbens alters metabolism in a distributed network of limbic and prefrontal brain regions.

To gain further insight into the physiological mechanisms of DBS, beyond regional perfusion and metabolism, neuroligand PET methods offer great potential to examine specific biochemical processes during DBS. The dopaminergic neuroreceptor system is of particular interest with DBS treatment of movement disorders. Several PET studies have been conducted to examine the dopaminergic system during DBS of the subthalamic nucleus: all three came to the conclusion that stimulation of the subthalamic nucleus does not significantly alter ^{11}C-raclopride binding to D2/D3 receptors in the striatum (caudate and putamen) (Abosch et al., 2003; Hilker et al., 2003; Strafella et al., 2003). However, another study reported significant ^{11}C-raclopride binding differences between pre- and post-DBS surgery groups, suggesting that DBS of the subthalamic nucleus reduces levadopa-induced fluctuations of synaptic dopamine levels in the striatum (Nimura et al., 2005). Despite its frequent usage in studying D2/D3 receptor binding, ^{11}C-raclopride, has limited sensitivity for regions outside of the striatum due to low specific-to-nondisplaceable binding ratios. ^{18}F-Fallypride is a high affinity D2/D3 radioligand (Mukherjee et al., 1999), providing favorable imaging characteristics in the extrastriatal regions of the brain and serves as a more useful radioligand for exploring system-wide changes in the dopaminergic network (Christian et al., 2000).

In this study, ^{18}F-fallypride was used to track changes in D2/D3 receptor binding as a result of DBS of the bed nucleus of the stria terminalis (BNST). Chronic stimulation of the BNST was explored as a mechanism for regulating the feeding habits of a naturally obese rhesus monkey. Previous work has shown that the BNST has projections to a variety of dopaminergic neurons (Fudge and Haber, 2001) and that lesions of limbic system components closely related to the BNST have lead to hyperphagia and obesity in rats (stria terminals (Rollins et al., 2006), posterior dorsal amygdala (King, 2006)). A reduction in D2/D3 receptor availability has been reported in obese humans, suggesting a deficiency in the modulating role of dopamine in motivational and reward systems in obese subjects (Wang et al., 2001). The BNST is implicated in modulating dopamine transmission in these systems (Norgren et al., 2006). We report on the utility of small animal PET for tracking neurochemical changes brought about by DBS.

2. Experimental procedures

2.1. DBS surgery and stimulation parameters

The experiment involved repeated scans of a male rhesus monkey (*macaca mulatta*: 6 years, 15 kg). Experimental procedures were approved by the UW Institutional Animal Care and Use Committee. Magnetic resonance imaging (MRI) images of the brain were acquired before and after surgery; pre-surgery images were used for surgical planning, post-surgery images for aiding in determination of the stimulated structure. The DBS lead was surgically implanted in the right bed nucleus of the stria terminalis (BNST), corresponding to the coordinates of $x = 3.3$ mm, $y = 3.85$ mm (posterior to the anterior commissure), $z = 0.55$ mm (above AC-PC plane) of the Paxinos et al. (2000) rhesus atlas. Electrode location was later confirmed based upon histological sections following the experiments. After surgery, the animal was allowed to recover for 2 months before the acquisition of the post-surgery MRI and PET scans.

The electrode waveform generator (located in the thorax) was set to deliver electrical pulses to the two most distal contacts of the electrode with a pulse width of 60 μs. Frequency was set to either 130 or 50 Hz using a pulse amplitude of 0.5, 1.0 or 2.0 V. These stimulation parameters were chosen because they are commonly used clinical stimulation patterns. As stimulation frequency has been shown to influence effectiveness of clinical DBS treatment (Moro et al., 2002; Windels et al., 2003), stimulation using both 130 and 50 Hz was applied to investigate the frequency dependence on BNST stimulation response.

2.2. Timing of PET scans and stimulation parameter changes

The timing of PET scans relative to stimulation voltage and frequency is shown in Fig. 1a. The first 130 Hz (high frequency) stimulation period consisted of 4 weeks of constant stimulation at 0.5 V followed by 4 weeks with the system turned off, during which service was performed on the waveform generator. After the service period, the stimulators were turned on again at 130 Hz; 4 weeks at 1.0 V and another 4 weeks at 2.0 V. Subsequently, the stimulator was turned off for 4 weeks (washout period), followed by 12 weeks of stimulation at 50 Hz. This 12-week low-frequency period was split into three 4-week segments with the voltage set to 0.5, 1.0 and 2.0 V, respectively. Following the 50 Hz period, the stimulator remained off for a second washout period. All PET scans were acquired within 5 days of the end of each time period. The final PET scan was acquired 4.5 weeks after 50 Hz stimulation ended.

2.3. Animal care procedures

To allow for accurate measurements of food intake, the animal was individually housed at the Wisconsin National Primate Research Center. Other monkeys were in adjacent cages as to minimize environmental effects. The room was maintained at a temperature of 21 °C with a 12-hr light/dark cycle. The animal was allowed *ad libitum* access to food for 8 hr/day starting at 8:00 am and water was continuously available. The caloric intake and weight of the subject were recorded throughout the course of the experiments.

On the day of each scan the monkey was anesthetized with ketamine (15 mg/kg) and transported from its home cage to the PET scanner. There was a period of greater than 50 min between administration of ketamine and the injection of radiotracer to minimize the potential effects on radioligand binding. Though the effects of ketamine on D2/D3 availability are small, approximately 2% (Nader et al., 1999; Nader and Czoty, 2008), this timing was recorded to examine potential confounding effects. Upon arrival at the PET scanner, the monkey was intubated and maintained under isoflurane at 0.75–1.5% for the duration of the scan. The monkey was positioned face-down in a custom-made head-holder mounted to the scanner bed, yielding repositioning accuracy on the order of several millimeters between PET scans. Body temperature was maintained using a warm air heater and a continuous i.v. infusion of saline was administered to prevent dehydration. Heart rate, breathing rate, body temperature, and SpO_2 were monitored and logged during the course of each PET scan.

2.4. PET scans

Following positioning, attenuation scans were acquired for 518 s using a Co-57 transmission point source. The dynamic emission PET

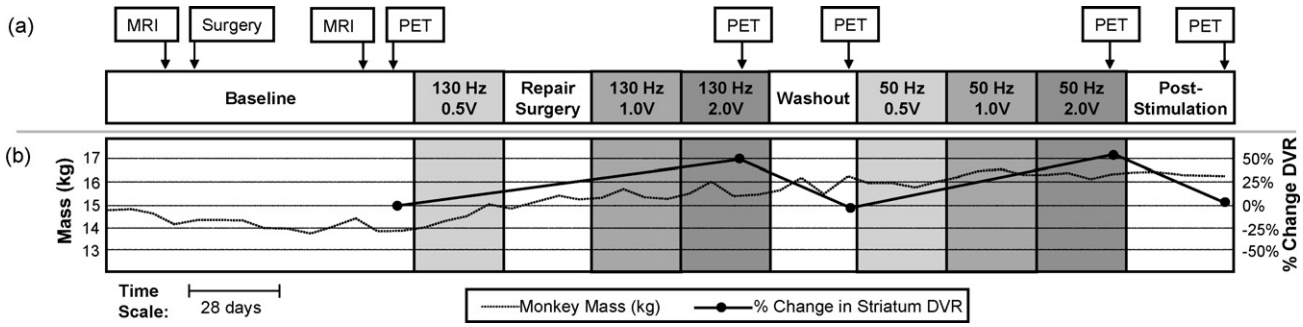

Fig. 1. (a) Timeline showing stimulation duration, strength, and frequency. Scanning times are indicated above the timeline. (b) Weight and striatum ^{18}F-fallypride DVR data are plotted below the timeline. Left axis is for monkey mass plot (dotted line). Right axis gives percent change over baseline in striatal DVR (solid line).

scan was initiated with the 30 s bolus i.v. infusion of ^{18}F-fallypride (5.12 ± 0.24 mCi, injected mass 0.05 ± 0.02 μg/kg) and data was acquired for 2.5 h on a Concorde microPET P4 scanner (Tai et al., 2001). Emission data was acquired in list mode for the duration of the scan. Following the scan, the animal was removed from the anesthesia, allowed to recover, and returned to the housing facilities.

For the final PET scan, the stimulator was activated (130 Hz, 2.0 V) 110 min after the injection of ^{18}F-fallypride and the scan was continued for an additional 70 min. This procedure was followed to investigate the possible acute effects of stimulator activation. The stimulator was turned off immediately following the emission scan. Toggling power to the stimulators was performed via a transcutaneous DBS programming device placed near the waveform generator, out of the field of view of the scanner. No motion in the animal was evident during the activation period.

2.5. Image processing

An attenuation sinogram was created using the segmented transmission scan. Emission listmode data for ^{18}F-fallypride were binned into 41 frames (frames × minutes per frame; 4×0.5, 5×1, 6×2, 5×3, 5×4, 15×6) making corrections for dead-time and randoms. The emission sinograms were reconstructed with filtered backprojection using a 0.3 cm^{-1} Hann filter, zoom of 1.5×, and $128 \times 128 \times 63$ voxel matrix size with voxel size of 1.26 mm × 1.26 mm × 1.21 mm. Corrections were made for attenuation, decay, scanner normalization, and scatter to create images with quantitative units of nCi/cc.

^{18}F-Fallypride binding was compared for all scans based on the measurement of the distribution volume ratio (DVR). Mathematically, DVR is described by the relationship, $\mathrm{DVR} = f_{\mathrm{ND}} B_{\mathrm{avail}}/K_{\mathrm{D}} + 1$, where B_{avail} is the density of receptors available for radioligand binding, f_{ND} is the free fraction in the nondisplaceable compartment, and K_{D} is the apparent (*in vivo*) dissociation rate constant (Innis et al., 2007). Parametric images of DVR were created using the multi-linear reference tissue model described previously (Ichise et al., 2003), using $t^* = 29$ min. The cerebellum was used as a reference region, representing *in vivo* kinetics in a brain region of negligible specific binding. Cerebellum time activity curves were obtained by drawing five 8.8 mm-diameter circles on each of three slices on the posterior cerebellum. For the generation of voxel-based parametric images, each frame of the dynamic images was smoothed using a 3-voxel (3.8 mm) FWHM 3D Gaussian kernel.

To account for the variability in positioning of the head-holder, FSL flirt (Smith et al., 2004) was used to register all images to a common space as defined by the pre-surgery MRI. This procedure involved the following steps: (1) registering each integrated PET scan to the T1-weighted MRI, (2) creating a PET template from an average of the coregistered PET images, and (3) registering each PET to the template image. Based on centroid matching in the striatum, the images were estimated to have sub-voxel alignment accuracy, which is expected for intrasubject, intramodal registrations (Woods et al., 1998). The transformations were then applied to the ^{18}F-fallypride DVR parametric images, putting all images (MRI, integrated PET and PET–DVR) into a common space, allowing for identical regions of interest (ROIs) to be applied to all images and facilitating voxel-based analyses. Similarly, to allow for comparison of time-activity curves, transformations and ROIs were applied to 4D dynamic PET data for both baseline and final scans.

ROIs were centrally placed within the boundaries of each region, defined on the MRI/PET coregistered images. The average value within each ROI is reported for DVR images as well as percent change from baseline. ROIs included (with volumes given) the left and right divisions of the caudate (0.16 cm^3 each), putamen (0.24 cm^3 each), substantia nigra (0.060 cm^3), the inferior-medial region of the thalamus (thalamus, 0.030 cm^3), and the prefrontal cortex (0.967 cm^3). Percent change in DVR is reported relative to baseline: [(scan − baseline)/baseline] × 100%. Voxel-based whole brain images of percent change from baseline DVR were created and examined for regional changes throughout the whole brain. Voxels with either the 'scan' or 'baseline' DVR value less than 1.0 were masked from these images. Assuming a constant ligand–receptor affinity, an increase in DVR (positive percent change) represents more available D2/D3 receptors, while a decrease in DVR (negative percent change) represents fewer available receptors.

To examine anterior–posterior changes within the striatum (investigated due to a visually apparent shift in binding in the 130 Hz study) we examined line profiles (3-voxel width) through the striatum on a single axial slice of the DVR images.

The ROI data for the acute DBS activation (final) study was analyzed using a modified model to detect the presence of time-dependent changes in radiotracer binding due to the activation of the electrode. For this experiment, the method described by Alpert and colleagues (Alpert et al., 2003) was used to account for time-varying changes in the kinetic parameters as expressed in the equation:

$$C(t) = RC_{\mathrm{r}}(t) + k_2 \int_0^t C_{\mathrm{r}}(u)\mathrm{d}u - \frac{k_2}{\mathrm{DVR}} \int_0^t C(u)\mathrm{d}u - \gamma \int_T^t \mathrm{e}^{-\tau(u-T)} C(u)\mathrm{d}u,$$

where $C(t)$ and $C_{\mathrm{r}}(t)$ are the specific binding tissue region and reference region radioactivity concentrations, respectively, at time t. R is the ratio of the delivery rate constants in the tissue and reference regions ($K_1/K_{1\mathrm{r}}$), k_2 is the tissue to plasma efflux constant in the tissue region. The γ term represents the temporal change

in the k_2/DVR parameter. The presence of endogenous neurotransmitter competition with the radioligand at the receptor sites would be reflected by a temporal change in DVR and is accounted for in the model with the $e^{-\tau(t-T)}$ term, at some time T. For this experiment, we have chosen T at the time of stimulator activation. The decay constant τ describes the rate at which this temporal variation discontinues and returns to baseline. Because the stimulator was activated for the remainder of the PET experiment, a value of $\tau = 0$ was chosen, thus keeping this term constant (rather than a decaying exponential). The baseline period (110 min) of the PET experiment provides sufficient data for estimating the parameters R, k_2 and k_2/DVR and the post-activation data (110–180 min) yields information for measuring γ. An increase in competing endogenous dopamine would result in $\gamma > 0$ whereas a decrease would result in $\gamma < 0$. Significance of the γ parameter was based upon the t-statistic calculated as γ/σ_γ; a threshold of $p < 0.05$ was selected as significant.

To serve as a comparison with the other PET scans, parametric images of ^{18}F-fallypride DVR were also created from this study based on the post hoc assumption that no DBS-induced change in binding occurred (i.e. null hypothesis that $\gamma = 0$). For this calculation, the identical model as used for the other PET scans was applied, using only the first 2.5 h of dynamic data for the estimation of DVR.

3. Results

During the course of the experiment there was an increase in the weight of the animal. The initial weight was 14.78 kg and final weight was 16.33 kg. Fig. 1b shows the time course of weight gain during the experiments. Pre-surgery baseline average daily caloric intake was 431 kcal/day. During stimulation periods daily caloric intake was 677 kcal/day (130 Hz) and 515 kcal/day (50 Hz). Washout and post-stimulation period averages were 579 kcal/day and 575 kcal/day, respectively.

Also shown in Fig. 1b is the change in striatal ^{18}F-fallypride DVR in relation to weight gain. ROI analyses revealed significant increases in DVR in all regions during both high and low frequency stimulation (Fig. 2) The striatal regions showed large increases while the extrastriatal regions showed modest to large increases during stimulation periods. For both washout and final scans (stimulators off), DVR values returned to near baseline DVR values; with the exception of the substantia nigra during the washout period (−17%) and both the PFC and thalamus post-stimulation (~20%). Comparisons of the left and right striatal regions revealed no significant asymmetries in DVR due to the unilateral stimulation.

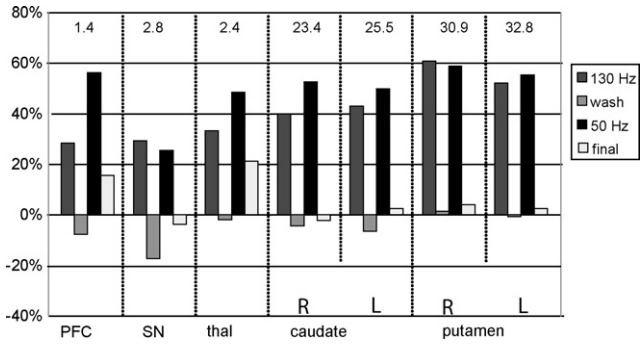

Fig. 2. ROI analysis: The regional changes in DVR over the course of the experiment. The bar graphs represent change in average DVR value within a ROI from baseline to the experimental scans ([scan − baseline]/baseline) × 100%. Values on top of graph represent baseline DVR value. PFC = prefrontal cortex, SN = substantia nigra, thal = thalamus.

A closer examination of the striatal region suggests a redistribution of available receptors within the striatum (Fig. 3). For 130 Hz stimulation, increases in DVR were greater in the anterior striatum than posterior, especially on the left side, resulting in a visually apparent shift of the region with highest DVR. The shift in binding is also illustrated in Fig. 4, where the long-axis profile reveals a bimodal shape for the 130 Hz scan.

The isocontours in Fig. 3 reveal the same pattern as seen in the ROI analysis of the caudate and putamen, with an increase in ^{18}F-fallypride DVR for both stimulation scans and a return to baseline DVR values during both the washout and post-stimulation periods. Fig. 5 highlights DBS-induced increases in DVR in the substantia

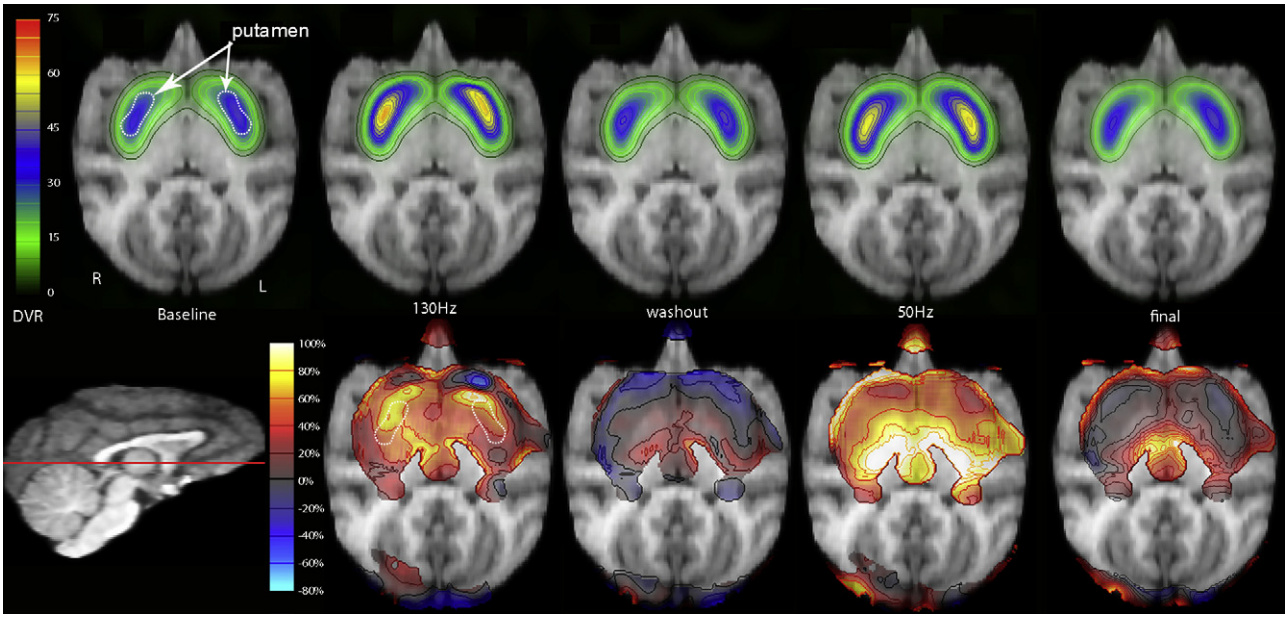

Fig. 3. Transaxial slices through the striatum as indicated in the midsagittal MRI (bottom left). In the top row, the color overlay indicates parametric images of ^{18}F-fallypride DVR (thresholded to include only striatum). The percent change in DVR (relative to baseline) is shown in the bottom row. Voxels with DVR < 1 in either 'baseline' or 'scan' were masked from the image. White dotted lines show the outline of the putamen ROI.

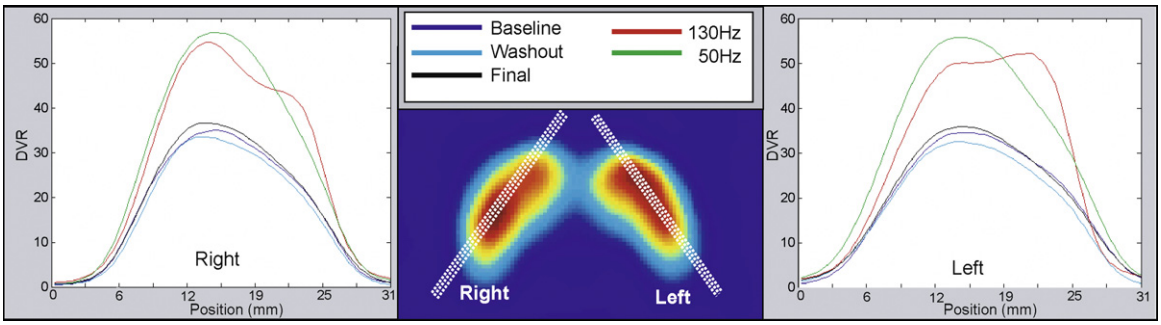

Fig. 4. Striatal profiles showing redistribution of ^{18}F-fallypride binding during 130 Hz stimulation. Profile lines are 3 voxels wide, as drawn on an axial slice 3 mm superior to those of Fig. 3. The *x*-axis represents position along profile line, with zero representing the lower portion of the profiles.

nigra region; showing a similar trend as seen in the striatum with changes most profound during the stimulation scans.

Time-activity curves of ^{18}F-fallypride in the caudate, putamen and substantia nigra for both baseline and the final scan are shown in Fig. 6. Kinetic analysis with the time-dependent term revealed no significance in the γ parameter, suggesting that acute changes in ^{18}F-fallypride binding are not present.

4. Discussion

There is a paucity of knowledge regarding the effect of DBS on the neuroreceptor systems in the brain. In this work, we chose to examine the dopamine system of a nonhuman primate due to its functional connections to the bed nucleus of the stria terminalis and the implicated role of dopamine in obesity and feeding patterns (Wang et al., 2002). ^{18}F-Fallypride was used as the PET radioligand due to its high selectivity for the D2/D3 receptors, favorable binding characteristics for measuring extrastriatal binding, and its suitability for translation to human studies. Considering the relatively non-invasive nature of the scanning protocol and that the stimulation parameters used in this experiment are similar to those used clinically, it is within reason that the methods used in this study could also be applied to humans with DBS electrodes in other brain regions.

Throughout both the striatal and extrastriatal regions of the brain we report large changes in ^{18}F-fallypride binding resulting from chronic simulation of the BNST. Because these studies were performed in a single animal, it is not possible to report statistical significance to the measured changes. However, comparison to intrasubject test–retest variability of 10% with ^{18}F-fallypride DVR in nonhuman primates (Christian et al., 2000) suggests that reported DVR changes in excess of 20% have a high likelihood of being due to the effects of DBS.

In research applications with reversibly bound PET neuroligands measuring group or drug effects, a change in DVR can be interpreted as (i) a change in the number of available receptors, B_{avail}, (ii) a change in the apparent dissociation rate constant (K_D) via a change in the concentration of competing endogenous neurotransmitter, or (iii) a combination of both (for review, see Laruelle, 2000). The nature of DBS in modulating neuronal firing combined with previous *in vivo* microdialysis work showing DBS modulation of neurotransmitter systems provides evidence that changes in DVR likely reflect alterations in competing endogenous neurotransmitter concentration (McIntyre et al., 2004).

Of great interest for this work are potential *decreases* in endogenous dopamine caused by DBS-induced inhibition of downstream circuits. A reduction in endogenous dopamine would produce more radiotracer binding and a positive change in DVR. Using pharmacologically-induced dopamine depletion, increases in bind-

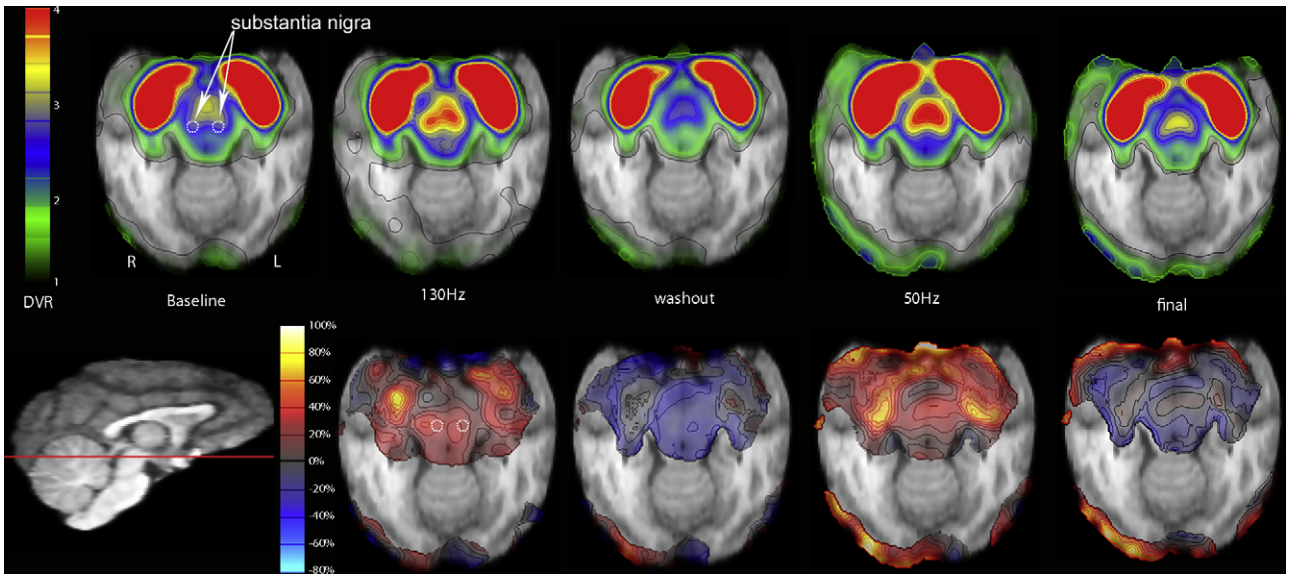

Fig. 5. Transaxial slices through the region of the substantia nigra (white arrow) as indicated by the midsagittal MRI (bottom, left). In the top row, the color overlay indicates parametric images of ^{18}F-fallypride DVR (thresholded to accentuate binding in the substantia nigra). The percent change in DVR (relative to baseline) is shown in the bottom row. Voxels with DVR < 1 in either 'baseline' or 'scan' were masked from the image. White dotted lines show the outline of the substantia nigra ROI.

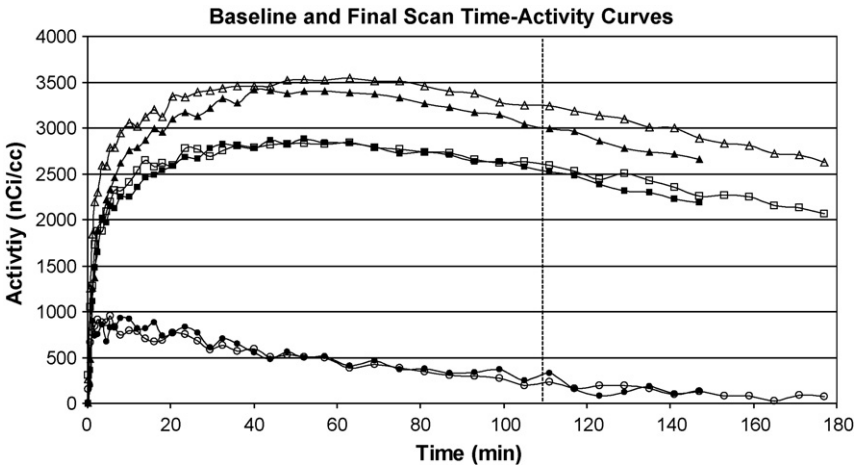

Fig. 6. Time-activity curves through the putamen (triangles), caudate (squares) and substantia nigra (circles) for both the baseline scan (filled points) and the final scan (open points). The DBS electrode was activated at 110 min, as indicated by the vertical dotted line.

ing potential (DVR-1) of 30–50% have been reported in nonhuman primates (Dewey et al., 1992; Ginovart et al., 1997), serving as an upper limit to changes in DVR due to competing endogenous dopamine. Because the results we observed were of this magnitude, we hypothesize that the reported changes are due to reduced competing dopamine, rather than an increase in the number of receptors.

Despite coming from only one animal, the changes in D2/D3 binding were profound, so we speculate on the cause of the observed changes. The alterations in the D2/D3 binding are likely to be caused by stimulation of the BNST, which has an influence over a variety of dopaminergic neurons, including a high density of projections to the substantia nigra (Fudge and Haber, 2001). If these projections were inhibited by the DBS, dopamine production of nigro-striatal neurons could have been shut down, leading to a decrease in striatal dopamine and the observed increases in DVR. Despite the large apparent decrease in striatal dopamine, the monkey did not show any change in control of movements. In the substantia nigra, the lower change in DVR could be the result of being under direct influence from the stimulated neurons. It is also possible that the D2/D3 autoreceptors in the substantia nigra (Tepper and Diana, 2002) are not as sensitive to endogenous dopamine as synaptic receptors in the other regions. Since DBS cannot deliver a uniform electric field across the entire target nucleus, different subregions of the BNST may have been stimulated to different degrees (McIntyre et al., 2004). This differential stimulation pattern may have been relayed through the substantia nigra to the striatum, leading to the observed change in striatal binding distribution during 130 Hz stimulation. It should not be expected that changes would be constrained to only the regions under direct stimulation or within 1–2 synapses of stimulated neurons, but also to any regions that are part of a larger neural circuit containing the nuclei or axons under direct stimulation (Montgomery and Gale, 2008). These higher degree connections may be responsible for the changes seen in regions such as the prefrontal cortex and the thalamus.

The final study did not detect any significant acute changes in ^{18}F-fallypride binding due to changes in endogenous dopamine. Visual inspection of the caudate and putamen time activity curves (Fig. 6) shows a subtle departure from the corresponding baseline data beginning at the DBS activation. However, the time-dependent term, γ, in the kinetic model could not sufficiently separate changes in specific binding from changes in radioligand delivery (via blood flow) due to the high correlation between parameters (Woods et al., 1998). While the methods used here did not detect a significant change, the prospects of measuring acute changes in dopamine release induced by DBS remain intriguing and warrant further investigation using methods with improved detection sensitivity, possibly characterizing both changes in magnitude and release timing (Morris et al., 2008).

Previous PET studies of neuroreceptor systems have not been able to demonstrate a significant change in ^{11}C-raclopride binding in humans as a result of DBS (Abosch et al., 2003; Hilker et al., 2003; Strafella et al., 2003). This lack of observed effect points to the limitations in conducting such experiments in subjects with severely degenerated nigro-striatal innervation and with limited ability to evoke a dopamine response. In this present study, all neurons under the influence of DBS are assumed to be healthy, functioning neurons with the capacity to modulate dopamine release, yielding the potential for measuring large changes in ^{18}F-fallypride binding. Furthermore, by choosing a high-affinity D2/D3 antagonist for the radiotracer, we were able to examine regions outside the D2/D3 receptor rich striatum, where the effects of DBS may play a prominent role.

Also of considerable interest is the positive correlation of striatal DVR with weight gain. While the monkey did gain weight over the period of the whole study, it was during the stimulation periods that most of the weight was gained. This was also the period of the largest increases in DVR. There was less weight gain during the washout and post-stimulation periods, both of which correspond to a return of DVR to baseline values. This observation is in line with previous findings that report a normalization of weight in obese mice following treatment with a dopamine D1/D2 agonist, SKF-38393 (Bina and Cincotta, 2000), so it follows that the reduction of endogenous dopamine reported herein may have played a role in the monkey's weight gain.

There is a wide range of additional studies that could be acquired on animals with DBS to provide a further understanding of the D2/D3 dopaminergic system changes during the DBS treatment. These include measurement at a variety of stimulation amplitudes and over a wider range of stimulation frequencies. Also of great interest would be a correlation of behavioral data with temporal changes in D2/D3 receptor binding following the initiation of simulation and after its termination, possibly providing insight into the receptor-dependent thresholds of DBS therapeutic effectiveness. Further studies are also warranted to uncouple the measurements of receptor density (B_{max}) and competing endogenous neurotransmitter (K_D) through the use of a multiple-injection experiment

(Christian et al., 2004). Such knowledge would aid in the understanding of changes at dopaminergic synapses during DBS which could lead to more effective clinical uses of DBS or as an inspiration for new experimental applications for DBS.

5. Conclusion

PET neuroligand imaging using ^{18}F-fallypride has demonstrated the sensitivity to track changes in dopamine D2/D3 binding during the course of deep brain stimulation of the BNST. The results show a profound change in ^{18}F-fallypride DVR due to stimulation of both 130 Hz and 50 Hz and a return to baseline DVR values when the stimulator was turned off during both washout and after stimulation. These methods show great potential for providing insight into the neurochemical mechanisms of DBS, and warrant further use of neuroligand PET imaging in deep brain stimulation research.

Acknowledgements

The authors would like to thank the following for their contributions to this research, making it possible: Wendy Newton and Vicky Carter for nonhuman primate handling and scheduling; Terry Oakes for help in image processing; as well as Dr. Erwin Montgomery and Dr. Ankur Garg for technical discussions and the journal reviewers. This material is based upon work supported in part by the Office of Research and Development, Rehabilitation R&D Service, Department of Veterans Affairs. N.T.V. was supported by NIH training grant T90 DK070079. The DBS electrodes were donated by Medtronic of Minneapolis, MN.

References

Abosch A, Kapur S, Lang AE, Hussey D, Sime E, Miyasaki J, et al. Stimulation of the subthalamic nucleus in Parkinson's disease does not produce striatal dopamine release. Neurosurgery 2003;53:1095–105.

Alpert N, Badgaiyan R, Livni E, Fischman A. A novel method for noninvasive detection of neuromodulatory changes in specific neurotransmitter systems. NeuroImage 2003;19:1049–60.

Bina KG, Cincotta AH. Dopaminergic agonists normalize elevated hypothalamic neuropeptide Y and corticotropin-releasing hormone, body weight gain, and hyperglycemia in ob/ob mice. Neuroendocrinology 2000;71:68–78.

Christian BT, Narayanan TK, Shi B, Mukherjee J. Quantitation of striatal and extrastriatal D-2 dopamine receptors using PET imaging of [18F]fallypride in nonhuman primates. Synapse 2000;38:71–9.

Christian BT, Narayanan T, Shi B, Morris ED, Mantil J, Mukherjee J. Measuring the in vivo binding parameters of [18F]-fallypride in monkeys using a PET multiple-injection protocol. J Cereb Blood Flow Metab 2004;24:309–22.

Dewey SL, Smith GS, Logan J, Brodie JD, Yu DW, Ferrieri RA, et al. GABAergic inhibition of endogenous dopamine release measured in vivo with 11C-raclopride and positron emission tomography. J Neurosci 1992;12:3773–80.

Fudge JL, Haber N. Bed nucleus of the stria terminalis and extended amygdala inputs to dopamine subpopulation in primates. Neuroscience 2001;104:807–27.

Fukuda M, Mentis MJ, Ma Y, Dhawan V, Antonini A, Lang AE, et al. Networks mediating the clinical effects of pallidal brain stimulation for Parkinson's disease: a PET study of resting-state glucose metabolism. Brain 2001;124:1601–9.

Ginovart N, Farde L, Halldin C, Swahn CG. Effect of reserpine-induced depletion of synaptic dopamine on [11C]raclopride binding to D2-dopamine receptors in the monkey brain. Synapse 1997;25:321–5.

Hamani C, McAndrews MP, Cohn M, Oh M, Zumsteg D, Shapiro CM, et al. Memory enhancement induced by hypothalamic/fornix deep brain stimulation. Ann Neurol 2008;63:119–23.

Haslinger B, Kalteis K, Boecker H, Alesch F, Ceballos-Baumann AO. Frequency-correlated decreases of motor cortex activity associated with subthalamic nucleus stimulation in Parkinson's disease. Neuroimage 2005;28:598–606.

Hilker R, Voges J, Ghaemi M, Lehrke R, Rudolf J, Koulousakis A, et al. Deep brain stimulation of the subthalamic nucleus does not increase the striatal dopamine concentration in parkinsonian humans. Mov Disord 2003;18:41–8.

Hilker R, Voges J, Weisenbach S, Kalbe E, Burghaus L, Ghaemi M, et al. Subthalamic nucleus stimulation restores glucose metabolism in associative and limbic cortices and in cerebellum: evidence from a FDG-PET study in advanced Parkinson's disease. J Cereb Blood Flow Metab 2004;24:7–16.

Ichise M, Liow JS, Lu JQ, Takano A, Model K, Toyama H, et al. Linearized reference tissue parametric imaging methods: application to [11C]DASB positron emission tomography studies of the serotonin transporter in human brain. J Cereb Blood Flow Metab 2003;23:1096–112.

Innis RB, Cunningham VJ, Delforge J, Fujita M, Gjedde A, Gunn RN, et al. Consensus nomenclature for in vivo imaging of reversibly binding radioligands. J Cereb Blood Flow Metab 2007;27:1533–9.

King BM. Amygdaloid lesion-induced obesity: relation to sexual behavior, olfaction, and the ventromedial hypothalamus. Am J Physiol Regul Integr Comp Physiol 2006;291:1201–14.

Lacan G, De Salles AAF, Gorgulho A, Krahl SE, Frighetto L, Behnke EJ, et al. Modulation of food intake following deep brain stimulation of the ventromedial hypothalamus in the vervet monkey. J Neurosurg 2008;108:336–42.

Laruelle M. Imaging synaptic neurotransmission with in vivo binding competition techniques: a critical revew. J Cereb Blood Flow Metab 2000;20:423–51.

Leone M, Franzini A, Broggi G, Bussone G. Expanding the role of deep brain stimulation from movement disorders to other neurological diseases. In: Freese A, Simeone FA, Leone P, Janson C, editors. Principles of Molecular Neurosurgery. Basel: Karger; 2005. p. 270–83.

Mayberg HS, Lozano AM, Voon V, McNeely HE, Seminowicz D, Hamani C, et al. Deep brain stimulation for treatment-resistant depression. Neuron 2005;45:651–60.

McIntyre CC, Savasta M, Walter BL, Vitek JL. How does deep brain stimulation work? Present understanding and future questions. J Clin Neurophysiol 2004;21:40–50.

Montgomery EB, Gale JT. Mechanisms of action of deep brain stimulation (DBS). Neurosci Biobehav Rev 2008;32:388–407.

Moro E, Esselin RJA, Hommel M, Benabid AL. The impact on Parkinson's disease of electrical parameter settings in STN stimulation. Neurology 2002;59:706–13.

Morris ED, Normandin MD, Schiffer WK. Initial comparison of ntPET with microdialysis measurements of methamphetamine-induced dopamine release in rats: support for estimation of dopamine curves from PET data. Mol Imaging Biol 2008;10:67–73.

Mukherjee J, Yang ZY, Brown T, Lew R, Wernick M, Ouyang X, et al. Preliminary assessment of extrastriatal dopamine D-2 receptor binding in the rodent and nonhuman primate brains using the high affinity radioligand, 18F-fallypride. Nucl Med Biol 1999;26:519–27.

Nader MA, Czoty PW. Brain imaging in nonhuman primates: insights into drug addiction. ILAR J 2008;49:89–102.

Nader MA, Grant KA, Gage HD, Ehrenkaufer RL, Kaplan JR, Mach RH. PET imaging of dopamine D2 receptors with [18F]fluoroclebopride in monkeys: effects of isoflurane- and ketamine-induced anesthesia. Neuropsychopharmacol 1999;21:589–96.

Nimura T, Yamaguchi K, Ando T, Shibuya S, Oikawa T, Nakagawa A, et al. Attenuation of fluctuating striatal synaptic dopamine levels in patients with Parkinson disease in response to subthalamic nucleus stimulation: a positron emission tomography study. J Neurosurg 2005;103:968–73.

Norgren R, Hajnal A, Mungarndee SS. Gustatory reward and the nucleus accumbens. Physiol Behav 2006;89:531–5.

Paxinos G, Huang XF, Toga AW. The rhesus monkey brain in sterotaxic coordinates. San Diego: Academic Press; 2000.

Perlmutter JS, Mink JW. Deep brain stimulation. Annu Rev Neurosci 2006;29:229–57.

Perlmutter JS, Mink JW, Bastian AJ, Zackowski K, Hershey T, Miyawaki E, et al. Blood flow responses to deep brain stimulation of thalamus. Neurology 2002;58:1388–94.

Rollins BL, Stines SG, King BM. Role of stria terminalis in food intake and body weight in rats. Physiol Behav 2006;89:139–45.

Sani S, Jobe K, Smith A, Kordower JH, Bakay RAE. Deep brain stimulation for treatment of obesity in rats. J Neurosurg 2007;107:809–13.

Schlaepfer T, Cohen M, Frick C, Kosel M, Brodesser D, Axmacher N, et al. Deep brain stimulation to reward circuitry alleviates anhedonia in refractory major depression. Neuropsychopharmacology 2007;33:368–77.

Smith SM, Jenkinson M, Woolrich MW, Beckmann CF, Behrens TE, Johansen-Berg H, et al. Advances in functional and structural MR image analysis and implementation as FSL. Neuroimage 2004;23(Suppl. 1):208–19.

Strafella AP, Sadikot AF, Dagher A. Subthalamic deep brain stimulation does not induce striatal dopamine release in Parkinson's disease. Neuroreport 2003;14:1287–9.

Tai C, Chatziioannou A, Siegel S, Young J, Newport D, Goble RN, et al. Performance evaluation of the microPET P4: a PET system dedicated to animal imaging. Phys Med Biol 2001;46:1845–62.

Tepper, J.M., Diana, M., Electrophysiological pharmacology of mesenchephalic dopaminergic neurons In: Chiara, editor. Dopamine in the CNS II. Springer, Berlin, Heidelberg, New York; 2002 [Chapter 13].

Wang GJ, Volkow ND, Logan J, Pappas NR, Wong CT, Zhu W, et al. Brain dopamine and obesity. Lancet 2001;357:354–7.

Wang G, Volkow ND, Fowler JS. The role of dopamine in motivation for food in humans: implications for obesity. Expert Opin Ther Targets 2002;6:601–9.

Windels F, Bruet N, Poupard A, Feuerstein C, Bertrand A, Savasta M. Influence of the frequency parameter on extracellular glutamate and γ-aminobutyric acid in substantia nigra and globus pallidus during electrical stimulation of subthalamic nucleus in rats. J Neurosci Res 2003;72:259–67.

Woods RP, Grafton ST, Holmes CJ, Cherry SR, Mazziotta JC. Automated image registration: I. General methods and intrasubject, intramodality validation. J Comput Assist Tomogr 1998;22:139–52.